

Cavity Ring Project Data Analysis

Annie Jihyun Park
ajpark@mpq.mpg.de

February 27, 2021

Introduction

We use the spatially dependent ac-Stark shift of the clock transition to map the intensity profile of the cavity lattices. This document summarizes the data analysis went into the cavity fringe project.

Contents

1	Clock excitation	1
1.1	Clock excitation without dephasing	1
2	Potential	2
2.1	Measurements	4
2.1.1	Gaussian intensity profile	4
2.1.2	Ground and excited state trap frequencies (α_g/α_e)	5
2.1.3	Absolute clock laser detuning	5
2.2	Cross-check	8
2.2.1	Discrepancies between total ac-Stark & Trap frequency measurements	8
3	Appendices	9
3.1	Magnetic field calibration	9
3.2	Clock laser waist calibration	10
3.3	Quadratic Zeeman Shift	10
3.4	Ac-Stark shift from the clock laser	10

1 Clock excitation

1.1 Clock excitation without dephasing

The clock transition ${}^1S_0 \leftrightarrow {}^3P_0$ is forbidden in even isotopes of alkaline-earth atoms due to the absence of hyperfine mixing (nuclear spin $I=0$). However, with a small external magnetic field, it is possible to induce the single-photon clock excitation by mixing 3P_0 and 1S_0 states ([4], Figure 1):

$$|{}^3P_0'\rangle = |{}^3P_0\rangle + \frac{\Omega_B}{\Delta_{32}} |{}^3P_1\rangle. \quad (1)$$

From [4], the rabi frequency Ω for the ${}^{88}\text{Sr}$ clock excitation is given by

$$\Omega = \langle {}^3P_0' | \hat{\mathbf{d}} \cdot \mathbf{E} | {}^1S_0 \rangle / \hbar = \frac{\Omega_L \Omega_B}{\Delta_{32}} \quad (2)$$

$$= \frac{\langle {}^3P_1 | \hat{\mu} \cdot \mathbf{B} | {}^3P_0 \rangle \langle {}^3P_1 | \hat{\mathbf{d}} \cdot \mathbf{E} | {}^1S_0 \rangle}{\hbar^2 \Delta_{32}} \quad (3)$$

$$= \frac{\langle \|\mu\| \rangle \langle \|d\| \rangle (\mathbf{E} \cdot \mathbf{B})}{\hbar^2 \Delta_{32}} \quad (4)$$

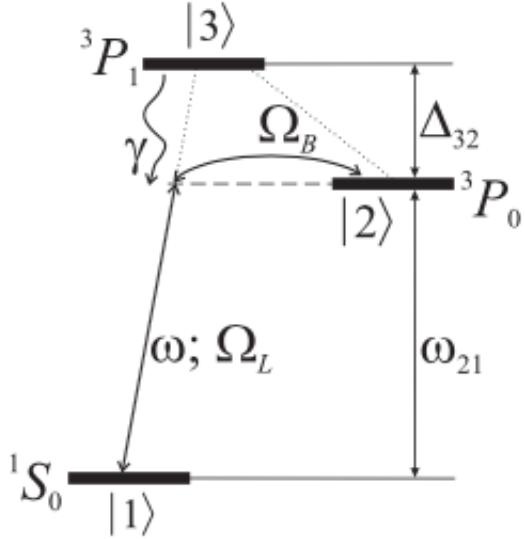


Figure 1: (Adopted from [4]) A small magnetic field breaks the LS coupling regime, and mixes $^3P_1(|3\rangle)$ and $^3P_0(|2\rangle)$ states, allowing otherwise forbidden transition from 1S_0 to 3P_0 .

where $\langle\|\mu\|\rangle$ and $\langle\|d\|\rangle$ are reduced matrix elements. Using $\langle\|\mu\|\rangle = \sqrt{2/3}\mu_B$ where μ_B is the Bohr magneton, $I = c\epsilon_0|E|^2/2$, and $\langle\|d\|\rangle=0.151$ [2], the rabi frequency can be expressed in terms of the applied fields and light intensity

$$\Omega = \alpha\sqrt{I}|\mathbf{B}|\cos\theta \quad (5)$$

where α is a measure of the induced Rabi frequency per unit of each of the fields, and I is the light intensity, θ is the angle between linearly polarized E and B fields. Alternatively, Ω can be expressed in terms of the induced field shifts, the quadratic Zeeman $\Delta_B = \beta\mathbf{B}^2$ and optical Stark $\Delta_L = \kappa I$ shifts where β and κ are respective shift coefficients, as

$$\Omega = \xi\sqrt{|\Delta_L\Delta_B|}\cos\theta \quad (6)$$

where $\xi \equiv \alpha/\sqrt{\beta\kappa}$.

2 Potential

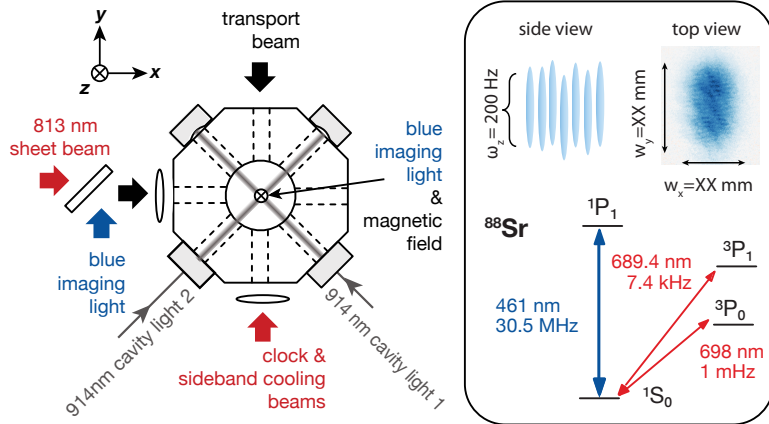


Figure 2: Optical setup

Our optical trap is generated by two-dimensional optical lattices created in the build-up cavities and a sheet-like dipole trap, as illustrated in Figure 2. Since the sheet beam is magic to the clock transition and its trap frequency is much smaller than the lattice trap frequencies (~ 200 Hz), we ignore the influence of the sheet beam for now. For the two-dimensional lattices, the potential is

$$\begin{aligned} U(x, y, z) &= U_0^x \left(\frac{w_0}{w(x)} \right)^2 e^{-2(y^2+z^2)/w_0^2} \cos^2(kx) + U_0^y \left(\frac{w_0}{w(y)} \right)^2 e^{-2(x^2+z^2)/w_0^2} \cos^2(ky) \\ &\stackrel{x,y \approx 0}{\approx} U_0^x e^{-2(y^2+z^2)/w_0^2} \cos^2(kx) + U_0^y e^{-2(x^2+z^2)/w_0^2} \cos^2(ky) \\ &\stackrel{U_x = U_y, z \approx 0}{\approx} U_0 \left(e^{-2y^2/w_0^2} \cos^2(kx) + e^{-2x^2/w_0^2} \cos^2(ky) \right), \end{aligned} \quad (7)$$

where $U_0^i = -\alpha_i I_0/(2c\epsilon_0)$, α_i is polarizability of a state i , and w_0 is the waist of the cavity mode. In Equation 7, we made the approximations $w_0/w(x) \approx 1$ and $e^{-2z^2/w_0^2} \approx 1$, which are valid because the Rayleigh range of the cavities modes are ~ 70 cm and the sheet confines the atoms at the gravity compensated position where $z \approx 60 \mu\text{m} \ll w_0$. The vibrational energy of the atoms trapped in the deep two-dimensional optical lattices [1] is

$$\begin{aligned} E_{n_x, n_y} &= h\nu_x(n_x + 1/2) - h\frac{\nu_{\text{rec}}}{2}(n_x^2 + n_x + 1) + h\nu_y(n_y + 1/2) - h\frac{\nu_{\text{rec}}}{2}(n_y^2 + n_y + 1) \\ &\stackrel{\nu_x = \nu_y}{=} h\nu + n_{xy}h\nu - h\frac{\nu_{\text{rec}}}{2}(n_x^2 + n_y^2 + n + 2) \end{aligned} \quad (8)$$

where n_i , ν_{rec} , and n_{xy} are vibrational mode along i axis, recoil frequency, and $n_x + n_y$, respectively. Following Equation 8, the energies of $n_{00} = 0$ or $n_{10} = 1$ (or $n_{01} = 1$) states are

$$E_{0,0} = h\nu - h\nu_{\text{rec}} \quad (9)$$

$$E_{1,0} = 2h\nu - 2h\nu_{\text{rec}} \quad (10)$$

$$\Delta E = h(\nu - \nu_{\text{rec}}).$$

So far, all the discussions have been the energies of a particular state in the trap. Now, let's look at the detuning required to drive the ground to excited states in the trap. This is particularly important for our purposes, since we are using this technique to characterize the cavity lattices. Since we are in non-magic lattices, we need to remember that the trap frequencies are different for the two states.

In free space, the energy difference between ${}^1\text{S}_0$ (g) and ${}^3\text{P}_0$ (e) states is $\Delta E_0 = \hbar\omega_0$. In non-magic lattices, there are additional energy shifts to consider: ac-Stark shift (ΔE_{ac}) and a shift due to the vibrational mode energy difference (ΔE_ν). Let's first consider the energy required to drive a carrier transition $n_{00}^g \leftrightarrow n_{00}^e$, where n_{jk}^i specifies vibrational mode jk of a state i ,

$$\begin{aligned} \Delta E &= \Delta E_0 + \Delta E_{\text{ac}} + \Delta E_\nu \\ &= \hbar\omega_0 + \frac{I(x, y)}{c\epsilon_0}(\alpha_g - \alpha_e) + h(\nu_e - \nu_g) \\ &\approx \hbar\omega_0 + \frac{I(x, y)}{c\epsilon_0}(\alpha_g - \alpha_e) + \sqrt{\frac{2h\nu_{\text{rec}}I(x, y)}{c\epsilon_0}}(\sqrt{\alpha_e} - \sqrt{\alpha_g}), \end{aligned} \quad (11)$$

where α_i and ν_i are the polarizability and trap frequency of a state i , respectively. To calculate ΔE_ν , we use Equation 9. In the last step, we use $\nu_i \approx 2\sqrt{\nu_{\text{rec}}|U_i|/h}$ where $U_i = -\alpha_i I(x, y)/2c\epsilon_0$, assuming the lattices with perfect contrasts. Rewriting Equation 11, the detuning required to drive a n_{00}^g to n_{00}^e is

$$\delta = \frac{\nu_g^2}{2\nu_{\text{rec}}} \left(1 - \frac{\alpha_e}{\alpha_g} \right) + \nu_g \left(\sqrt{\frac{\alpha_e}{\alpha_g}} - 1 \right) \quad (12)$$

or writing in terms of ν_e instead, one arrives at

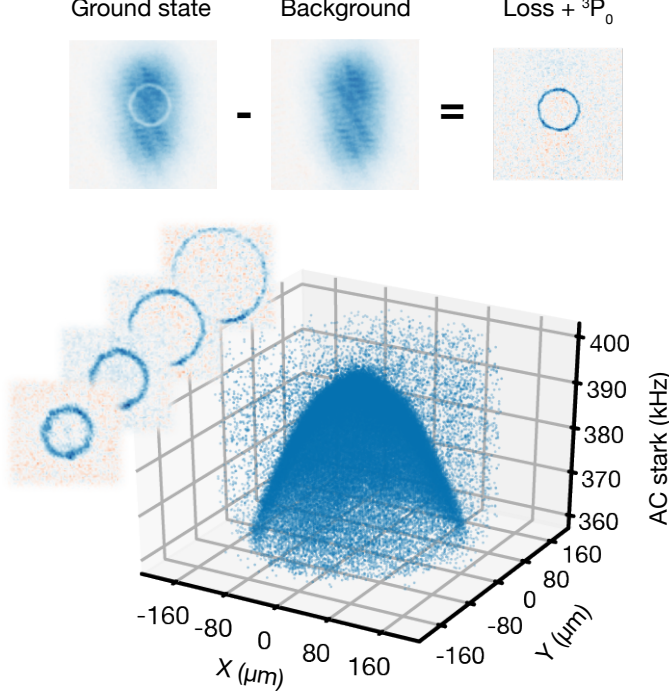


Figure 3: Reconstructed potential map (the quality of the figure is not great, will be updated later)

$$\delta = \frac{\nu_e^2}{2\nu_{\text{rec}}} \left(\frac{\alpha_g}{\alpha_e} - 1 \right) + \nu_e \left(1 - \sqrt{\frac{\alpha_g}{\alpha_e}} \right). \quad (13)$$

We can also look at ΔE required to drive a sideband transition $n_{ii}^g \leftrightarrow n_{i,i+1}^e$

$$\begin{aligned} \Delta E &= \Delta E_0 + \Delta E_{\text{ac}} + \Delta E_\nu \\ &= \hbar\omega_0 + \frac{I(x, y)}{c\epsilon_0} (\alpha_g - \alpha_e) + h(\nu_e - \nu_{\text{rec}}) \\ &\approx \hbar\omega_0 + \frac{I(x, y)}{c\epsilon_0} (\alpha_g - \alpha_e) + h \left(\sqrt{\frac{2\nu_{\text{rec}} I(x, y)}{c\epsilon_0 h}} - \nu_{\text{rec}} \right), \end{aligned} \quad (14)$$

where, again, the perfect contrast lattice assumption has been made in the last step.

2.1 Measurements

2.1.1 Gaussian intensity profile

We can reconstruct the two-dimensional potential map as shown in Figure 3 (will skip going into the details, since most of us are familiar with it). The fit function for the potential can be derived from Equation 11. So far, we have been neglecting E_v term in Equation 11 for the fit, since $E_v \ll E_{\text{ac}}$ (~ 10 kHz $\ll 400$ kHz). Neglecting E_v term, the fit function is

$$\delta(x, y) = \frac{\delta_{\text{tot}}}{2 + \epsilon} \left(e^{\frac{-2x}{w_0^2}} + (1 + \epsilon) e^{\frac{-2y}{w_0^2}} \right)$$

where ϵ characterizes the imbalance between the two orthogonal lattice axes' trap depths. The variables of the fit are the cavity mode waist w_0 and ϵ . The total detuning δ_{tot} can be extracted separately from the ground or excited state trap frequency measurements (subsection **Ground and excited state trap frequencies** (α_g/α_e)) or by beating the frequency comb and the clock laser (subsection **Absolute clock laser detuning**).

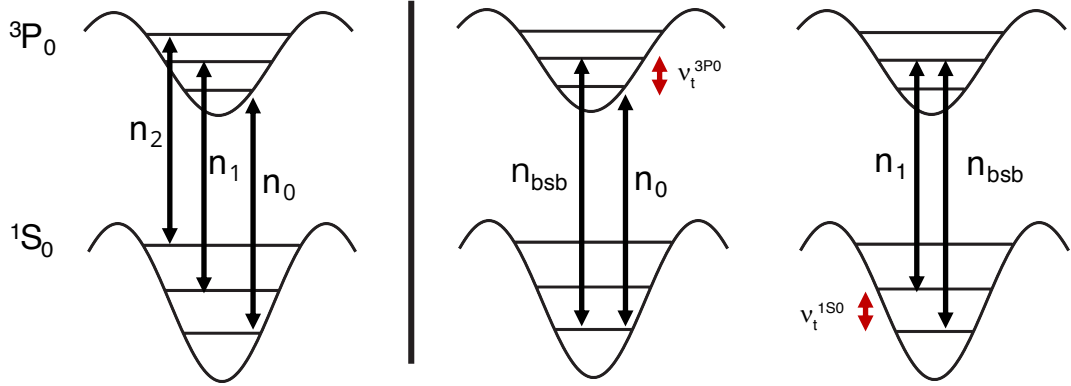


Figure 4: Carrier transitions are resolved (left) and by combining carrier and sideband transitions, one can find out ground and excited trap frequencies (right two pictures)

2.1.2 Ground and excited state trap frequencies (α_g/α_e)

In two-dimensional lattices which are not magic for the ${}^1\text{S}_0$ (g) and ${}^3\text{P}_0$ (e) states, the carrier transitions are resolved. As illustrated in Figure 4, by subtracting the carrier ($n_{00}^g \leftrightarrow n_{00}^e$ or $n_{11}^g \leftrightarrow n_{11}^e$) and blue sideband ($n_{00}^g \leftrightarrow n_{10}^e$) transition frequencies, we can find ground and excited state trap frequencies. This can be easily derived from Equation 9 and 10

$$\begin{aligned}\Delta f_{00,10} - \Delta f_{00,00} &= (E_{1,0}^e - E_{0,0}^g)/h - (E_{0,0}^e - E_{0,0}^g)/h \\ &= (2\nu_e - 2\nu_{\text{rec}} - \nu_g + \nu_{\text{rec}}) - (\nu_e - \nu_{\text{rec}} - \nu_g + \nu_{\text{rec}}) \\ &= (2\nu_e - \nu_g - \nu_{\text{rec}}) - (\nu_e - \nu_g) \\ &= \nu_e - \nu_{\text{rec}}\end{aligned}$$

and

$$\begin{aligned}\Delta f_{00,10} - \Delta f_{11,11} &= (E_{1,0}^e - E_{1,0}^g)/h - (E_{1,0}^e - E_{1,0}^g)/h \\ &= (2\nu_e - 2\nu_{\text{rec}} - \nu_g + \nu_{\text{rec}}) - (2\nu_e - 2\nu_{\text{rec}} - 2\nu_g + 2\nu_{\text{rec}}) \\ &= (2\nu_e - \nu_g) - (2\nu_e - 2\nu_g) \\ &= \nu_g - \nu_{\text{rec}},\end{aligned}$$

where $f_{ij,kf}$ is the transition frequency from $n_{ij}^g \leftrightarrow n_{kf}^g$. Figure 5 shows the carrier and sideband spectra for 2 by 2 averaged pixels. From the Lorentzian fits, we can find out $\Delta f_{00,00}$, $\Delta f_{11,11}$, and $\Delta f_{00,10}$. By subtracting the correct pairs, we can find out the polarizability ratio

$$\frac{\alpha_g}{\alpha_e} = \left(\frac{\Delta f_{00,10} - \Delta f_{11,11} + \nu_{\text{rec}}}{\Delta f_{00,10} - \Delta f_{00,00} + \nu_{\text{rec}}} \right)^2. \quad (15)$$

Equation 15 was confirmed numerically (based on Sebastian's python code: lattice_rings.py). The result is shown on the left in Figure 6, which clearly depicts that our estimation is susceptible to systemic errors. Ideally one would expect a flat distribution of the ratio across the sample; however, the ratio increases with the distance from the central pixel. So far, we are not sure what the cause is. If we ignore this systemic effect and restrict the estimation in a smaller central region (left on Figure 6), the noise distribution seems random. In this central area, the estimated ratio is **1.179 ± 0.002** .

2.1.3 Absolute clock laser detuning

We measure the absolute clock laser detuning required to address the atoms in the center of the lattices by beating the frequency comb with the clock laser. The expected detuning as a function of trap frequency (intensity) is expressed in Equation 12 and 13 (Equation 11). The clock laser beam path is splitted into

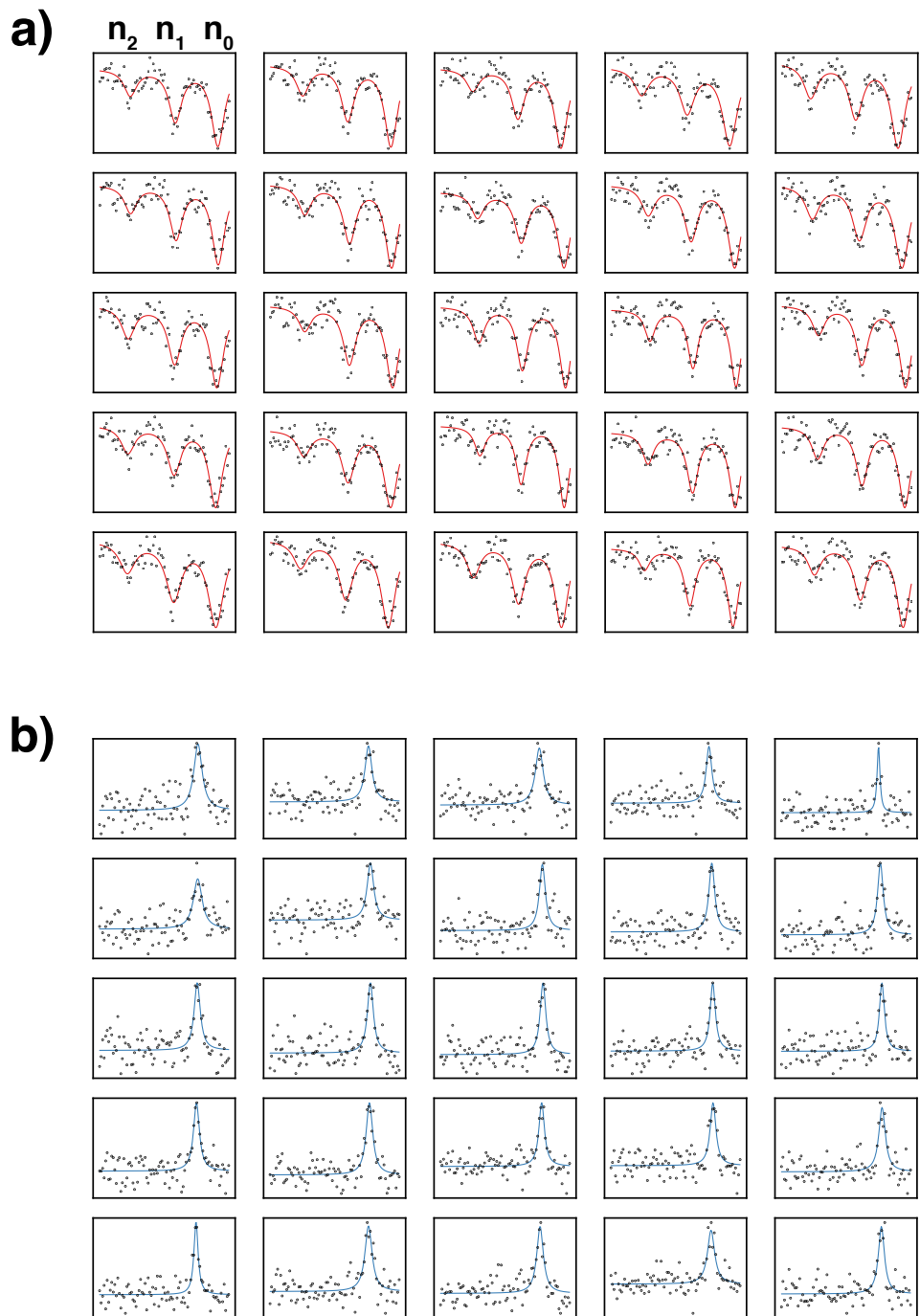


Figure 5: Carrier sideband spectra, data folder: \data _2020\10\29\it_sr88_clock_fringe
 $\text{arm1}=1.175V$ _arm2_0.975V_z_cooling_2 & it_sr88_clock_fringe_arm1=1.175V_arm2_0.975V_blueSideband_fine

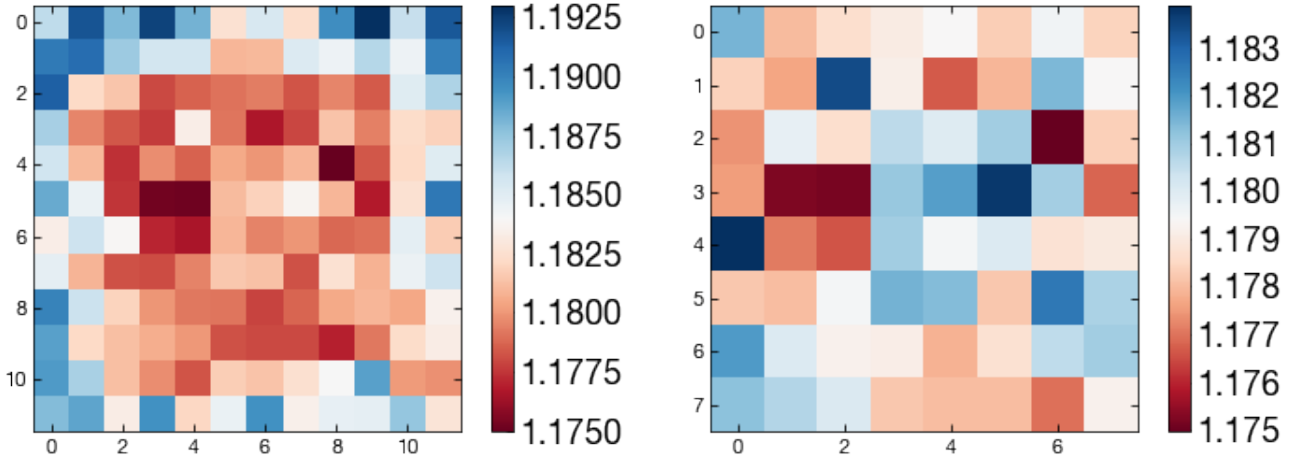


Figure 6: Polarizability α_g/α_e ratio for (a) larger size (b) smaller size

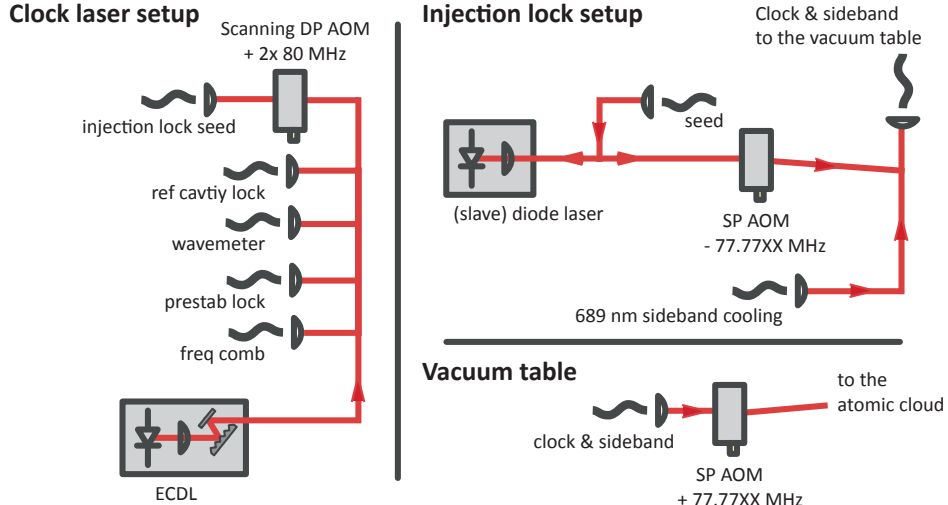


Figure 7: Clocklaser setup

multiple paths as shown in Figure 7, one of the paths is fiber coupled to the frequency comb setup, and the other path goes through a scanning double pass (DP) aom and then, fiber coupled to seed the injection lock. The output of the injection is used to probe the atoms.

To measure the maximum light shift, we scanned the double pass aom frequency to excite the center of the lattices. We repeated these measurements for two different trap frequencies. Figure 8 shows the carrier and blue sideband spectra. Taking each spectrum takes about half an hour to an hour, and after each carrier scan, we recorded the beat frequency recorded on the counter to find out the absolute ac-Stark shift.

The detunings with respect to the known $^{88}\text{Sr } ^1\text{S}_0 - ^3\text{P}_0$ transition frequency [3] were,

- (399533 ± 400) Hz for "high depth"
- (195385 ± 400) Hz for "half depth"

We know that the clock laser drifts about -400 Hz per hour. During the carrier frequency measurements, the DP aom frequency has been compensating for the drift, whereas the fiber port that was used for the beat does not go through this DP aom, thus, susceptible for the drift. If we include this shift,

- $(399533 \pm 400 + 400)$ Hz for "high depth"

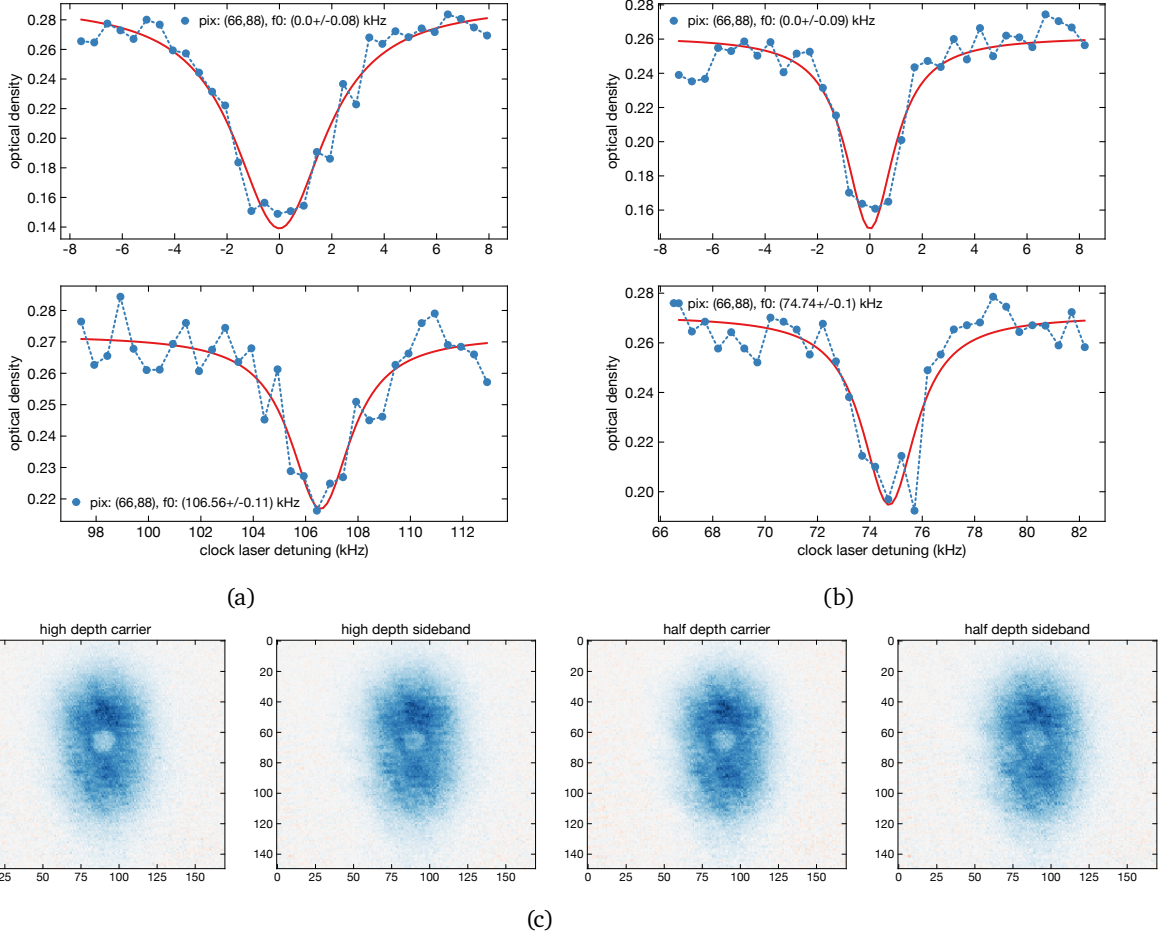


Figure 8: (a) carrier (top) and sideband (bottom) clock spectra of ground and excited states of high depth (b) same as (a) for half of the depth (c) in-situ $^1\text{S}_0$ images at the center frequency of carrier and sideband spectra (data folder: \data_2020\12\02\it_sr88_absolute_ac_stark)

- $(195385 \pm 400 + 400)$ Hz for "half depth"

Quadratic zeeman shift is about ~ 1 kHz at 50 G that was used for the measurements.

2.2 Cross-check

2.2.1 Discrepancies between total ac-Stark & Trap frequency measurements

We compare the measured polarizability ratio with the ratio derived using Marianna's polarizability values, which are (261.09 ± 1.16) a.u. at 914.0 nm and (260.91 ± 1.16) a.u. at 915.0 nm for α_g , and (220.8 ± 2.3) a.u. at 914.332 nm for α_e . To find out the α_g at 914.332 nm, I do linear interpolation and get (261.03 ± 0.87) at 914.332 nm. The comparisons with our measurement and Marianna's number are shown in Figure 9 on left.

From the extracted ratio, we can cross check whether the comb measurement in Section 2.1.3 agrees with the trap frequency measurements performed on the same day (Figure 8 (a) and (b)). For this cross check, we compare the total detuning δ_{tot} from the comb against the one derived from Equation 13:

$$\delta_{\text{tot}} = \underbrace{\frac{\nu^2}{e}}_{\text{data: Fig. 8}} \left(\underbrace{\frac{\alpha_g}{\alpha_e}}_{\text{data: Fig. 5}} - 1 \right) + \underbrace{\frac{\nu_e}{e}}_{\text{data: Fig. 8}} \left(1 - \underbrace{\sqrt{\frac{\alpha_g}{\alpha_e}}}_{\text{data: Fig. 5}} \right).$$

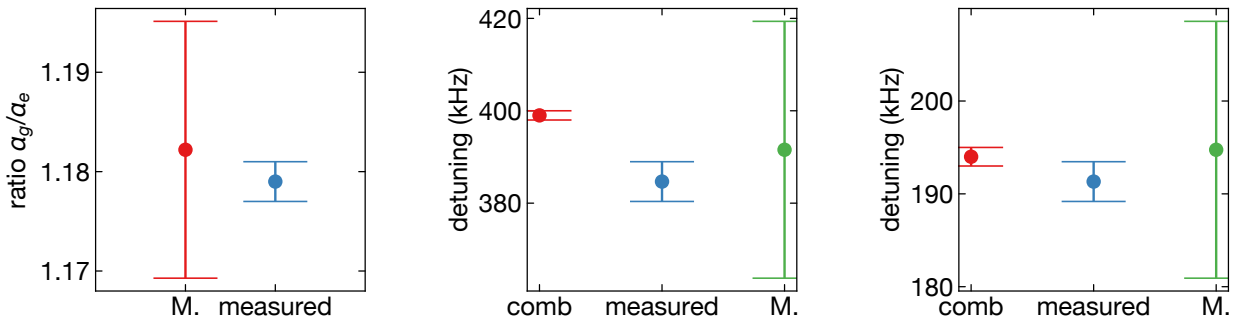


Figure 9: (left) polarizability ratio (α_g/α_e) comparison: M (Marianna's number) and measured (middle): δ_{tot} comparison for the "high depth" data (right) δ_{tot} comparison for the "half depth" data

The result is shown in Figure 9, which shows the discrepancies between the two results. Yet, we are not sure where the discrepancy is coming from.

Can we extract α_g ? The answer is no. From the two separate data sets, we extracted the polarizability ratio (α_g/α_e) and δ_{tot} at a particular ν_e . It seems that by using Equation 13, we should be able figure out α_g or α_e . However, we cannot because the trap frequency depends on two parameters, polarizability and intensity ($I(x, y)$):

$$\nu_i = 2 \sqrt{\frac{\nu_{\text{rec}} \alpha_i I(x, y)}{2c\epsilon_0}}.$$

Without a good knowledge of intensity, one cannot extract the polarizability.

3 Appendices

3.1 Magnetic field calibration

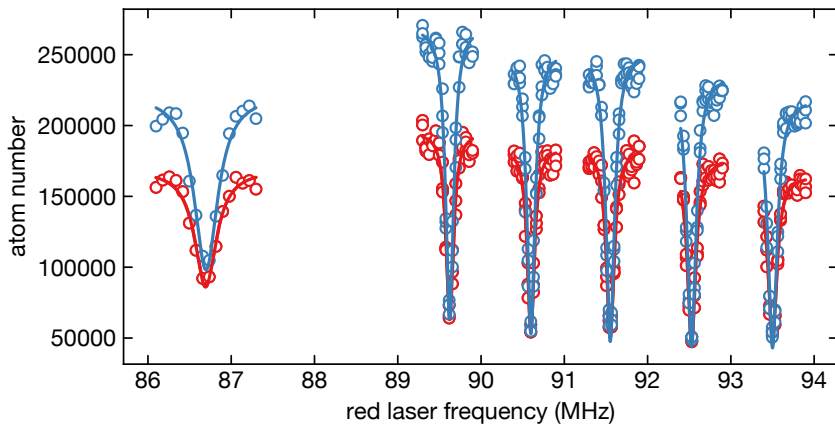


Figure 10: $^3\text{P}_1 m=1$ transition frequency shift as a function of field set voltage datapath:\data_2020\10\26\it_field_calibration

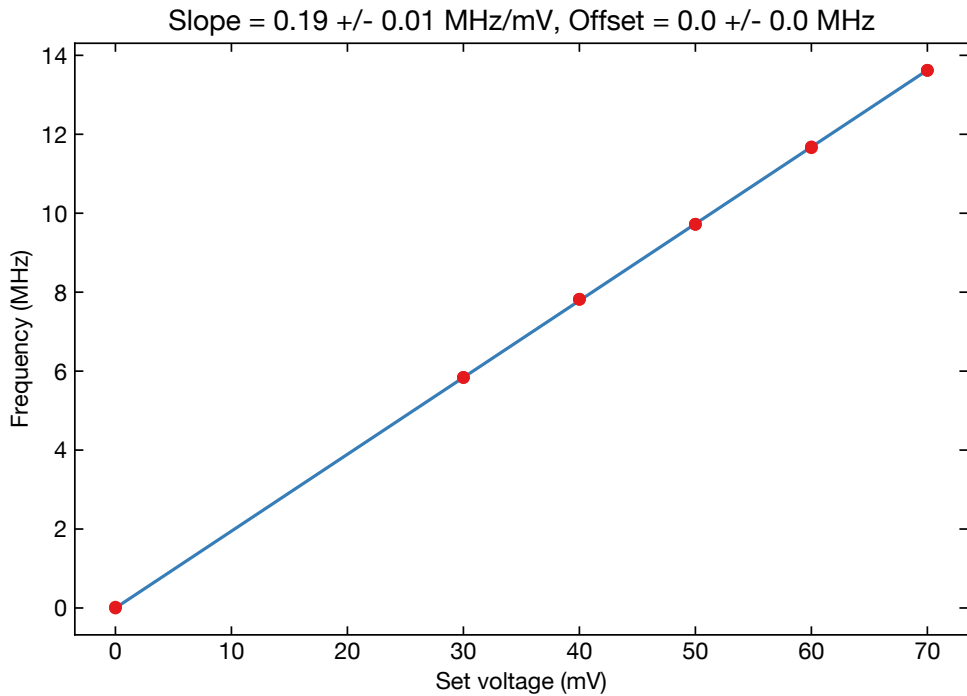


Figure 11: field calibration curve

3.2 Clock laser waist calibration

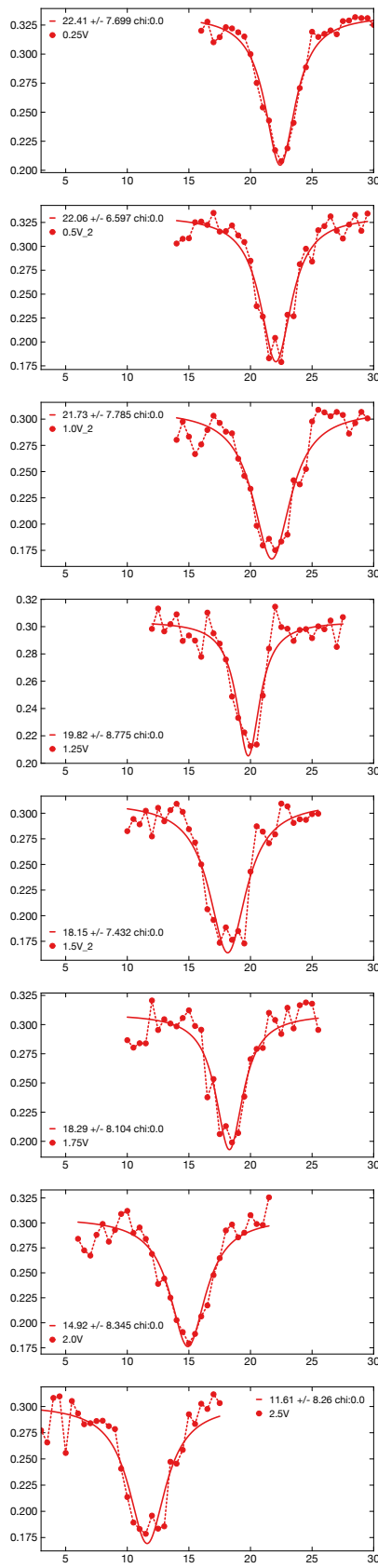
3.3 Quadratic Zeeman Shift

3.4 Ac-Stark shift from the clock laser

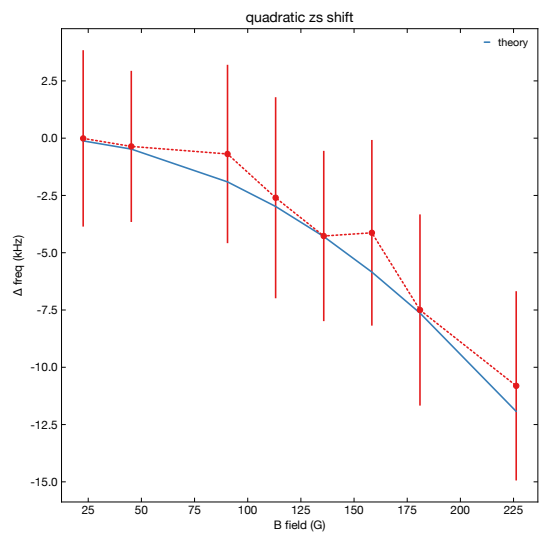
very small

References

- [1] S. Blatt, J. W. Thomsen, G. K. Campbell, A. D. Ludlow, M. D. Swallows, M. J. Martin, M. M. Boyd, and J. Ye. Rabi spectroscopy and excitation inhomogeneity in a one-dimensional optical lattice clock. *Phys. Rev. A*, 80:052703, 2009.
- [2] Alexandre Cooper, Jacob P. Covey, Ivaylo S. Madjarov, Sergey G. Porsev, Marianna S. Safronova, and Manuel Endres. Alkaline-earth atoms in optical tweezers. *Phys. Rev. X*, 8:041055, Dec 2018.
- [3] J. E. Sansonetti and G. Nave. Wavelengths, transition probabilities, and energy levels for the spectrum of neutral strontium (Sr I). *J. Phys. Chem. Ref. Data*, 39:033103, 2010.
- [4] A. V. Taichenachev, V. I. Yudin, C. W. Oates, C. W. Hoyt, Z. W. Barber, and L. Hollberg. Magnetic field-induced spectroscopy of forbidden optical transitions with application to lattice-based optical atomic clocks. *Phys. Rev. Lett.*, 96:083001, Mar 2006.



(a) clock resonant frequency shift for different field



(b) Quadratic zeeman shift

Figure 12